Dalton Transactions

ROYAL SOCIETY OF CHEMISTRY

PAPER

View Article Online
View Journal | View Issue

Cite this: *Dalton Trans.*, 2025, **54**, 8972

Cadmium sulfide quantum dots functionalized with serine, proline, and aspartic acid homologs to study the influence of ligand size on the induced circular dichroism†

Milan Balaz, *[a] Yoonbin A. Joh [b] and Krisztina Varga *[b]

Chirality, a fundamental property of molecules and materials, underlies numerous critical chemical, biochemical, and optical phenomena. Chiral organic molecules, termed capping ligands, have been shown to induce chirality in intrinsically achiral nanomaterials through electronic and structural interactions, as evidenced by the emergence of a circular dichroic (CD) signal. The sign and intensity of the CD spectra have been demonstrated to reflect both the ligand's absolute configuration and its binding geometry that could be tuned by solvent, temperature, base, countercation, and ligand's concentration. To gain a deeper understanding of ligand-induced chirality and facilitate the rational design of chiral materials, it is crucial to investigate the interplay between molecules and nanomaterials at the solid–liquid interface. In this study, we investigate the influence of capping ligand size on the induced CD spectra of colloidal cadmium sulfide quantum dots (CdS QDs) by using homologous pairs of amino acids: serine-homoserine, proline-homoproline, and aspartic-glutamic acids. In parallel, we explore the impact of a third functional group (attached to the achiral carbon) and the distance between the anchoring carboxylate group and this third functional group using spectroscopic techniques. Our findings highlight the significant role of ligand molecular structure and footprint (steric demand) on the induced CD signal of semiconductor nanoparticles. This study further emphasizes the importance of circular dichroism spectroscopy in probing surface binding geometry, ligand surface orientation, and ligand-nanocrystal hybridization.

Received 1st April 2025,
Accepted 7th May 2025

DOI: 10.1039/d5dt00778j

rsc.li/dalton

1. Introduction

The interfaces between molecules and inorganic materials are an active area of research with two major complementary objectives: understanding how molecules can induce and modulate the properties of inorganic materials, and conversely, how inorganic materials can be used to chemically transform or detect molecules. Chirality is a key property of molecules and materials and is behind several important processes and phenomena such as (bio)molecular recognition and folding, conductivity and mechanical strength, stereoselective synthesis and catalysis, and the interaction of light with matter (optical activity and chiroptical properties). Chiral inorganic quantum dots (QDs) are semiconductor nanocrystals, often functionalized with chiral molecules, that exhibit chiroptical properties such as circular dichroism (CD) and circularly polarized luminescence (CPL). While chiral QDs were initially synthesized in aqueous solutions from metal salts and chiral capping ligands (an approach pioneered by Gun'ko and coworkers),[1] a more robust and versatile method was developed later and involves chirality transfer *via* post-synthetic ligand exchange.[2,3] This process replaces achiral ligands on preformed achiral QDs with chiral ligands and is often facilitated by phase-transfer conditions. A variety of chiral nanoarchitectures, including chiral quantum dots (QDs), quantum rods, dot-in-rods, and nanoplatelets, have been prepared using ligand exchange. These materials have shown significant potential in sensing, biorecognition, catalysis, circularly polarized luminescence (CPL) emission, and spintronics.[4–17]

Spectroscopic, structural, and computational studies suggest that induced CD signal arises from either hybridization between achiral QD and chiral electronic states of ligands and/or chiral distortion of the QD lattice induced by

[a]*Integrated Science and Engineering Division, Underwood International College, Yonsei University, Seoul, Republic of Korea. E-mail: mbalaz@yonsei.ac.kr*
[b]*Department of Molecular, Cellular, and Biomedical Sciences, University of New Hampshire, Durham, NH, USA. E-mail: krisztina.varga@unh.edu*

† Electronic supplementary information (ESI) available. See DOI: https://doi.org/10.1039/d5dt00778j

the chiral ligands. The CD sign and CD anisotropy are determined by the chiral ligand's absolute configuration and chemical structures as well as the structure of native achiral ligands, which collectively define the chiral ligand binding geometry and ligand–ligand binding pattern (*i.e.*, footedness).[18–28] Studies utilizing the most common chiral capping ligands such as chiral thiols, carboxylic acids, and amino acids led to several key discoveries in water-soluble and organic-soluble QDs and paved ways to tune the CD characteristics of nanomaterials. Adding a new stereogenic center in the chiral ligand led to either increase or decrease of CD anisotropy depending on the match-mismatch of the new stereocenter with already present stereocenter.[29,30] Acetylation of the amino group of cysteine, use of different native 'growth' ligands (*e.g.*, oleic acid *vs.* tetradecylphosphonic acid), use of different countercations (tetrabutylammonium *vs.* ammonium), alpha-substituents (phenyl *vs.* hydroxy) or solvents (acetonitrile *vs.* formamide) were shown to cause induction of mirror image CD spectra, suggesting mirror-image surface binding orientations.[18,31–34] Capping ligand's concentration led to different binding geometries thus impacting the magnitude of induced CD bands.[35,36] The interplay between polar chiral ligands and non-polar achiral ligands on QDs not only tuned the CD spectra but also enabled the first synthesis of chiral QDs soluble in aprotic, non-polar solvents (*e.g.*, cyclohexane and hexane).[32,37] Spontaneous reorganization of the ligand binding geometry and orientation resulted in a change, or even an inversion, of the CD signal.[37–39] However, a comprehensive understanding enabling the rational design of chiral QDs remains elusive. Herein, we explore the effect of capping ligand molecular size and the role of the third functional group (not directly attached to the stereogenic carbon) on the induced chiroptical properties of CdS QDs using homologous amino acid pairs (*i.e.*, amino acids differing by a single methylene group [–CH_2–]; Chart 1). Our data demonstrate that both the size of the capping ligand, the presence of a third electron-donating functional group and its distance from the anchoring carboxylate group all contribute to the shape and anisotropy of the induced CD signal. They also emphasize the importance of CD spectroscopy in studies of molecular-material interface.

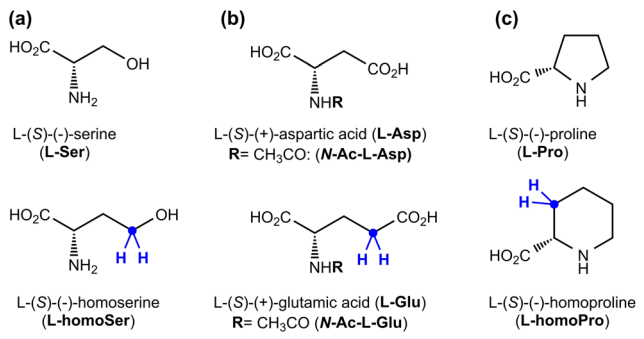

Chart 1 Chiral homologous amino acid capping ligands: (a) L-serine and L-homoserine, (b) L-aspartic acid, L-glutamic acid and their acetylated counterparts, and (c) L-proline and L-homoproline.

2. Experimental section

2.1 Materials

L- and L-Carboxylic acids and tetramethylammonium hydroxide (TMAH) were purchased from Sigma-Aldrich or P212121, LLC. Methanol was purchased from Fisher Scientific. All commercial chemicals were used as received. OA-CdS QDs were purchased from NNCrystal US Corporation or prepared by previously reported procedure.[29] The diameter of the CdS QDs was determined from the UV-vis absorption spectra.[40]

2.2 Phase transfer ligand exchange

Chiral CdS QDs have been synthesized by phase transfer ligand exchange as reported previously.[29] Briefly, chiral carboxylic acid and TMAH were dissolved in methanol and cyclohexane was added. The mixture was then deoxygenated under vigorous stirring using three vacuum-then-N_2 cycles. A cyclohexane solution of oleic acid capped CdS QDs (OA-CdS QDs) was added *via* a syringe to the deoxygenated stirred mixture. The resulting reaction mixture was vigorously stirred at RT under N_2 in the absence of light for 30 min. The reaction mixture was then left to stand for 30 min to allow the cyclohexane-methanol phases to fully separate after which the methanol layer was removed with a syringe. Quantitative yield (>90%) of chiral ligand capped CdS QDs has been confirmed by UV-vis spectroscopy. The properties of QDs functionalized with chiral acids were characterized (see ESI†).

3. Results and discussion

Chiral CdS QDs functionalized with homologous amino acid have been prepared as methanol solutions from cyclohexane solution of colloidal OA-CdS QDs with cubic blende structure (419.4 nm; $\varnothing_{CdS}$ = 4.1 nm, calculated from the UV-Vis spectra; Fig. S1 and 2†) following a previously reported procedure.[29,32] The ligand exchange process, as confirmed by UV-Vis absorption spectroscopy, replaced the achiral oleic acid on cadmium sulfide nanoparticles with homologous amino acids within 30 minutes, achieving a CdS recovery rate >90% (see ESI† for experimental conditions). Notably, all amino acid-capped CdS QDs displayed excellent colloidal stability and were used directly as their methanol solutions containing tetramethylammonium hydroxide, eliminating the need for precipitation, washing, or resuspension steps. Amino acids primarily bind to the QD surface *via* their carboxylate group (C1 carbon) as the anchoring point.[19,25,41–44] The appearance of an induced CD signal in the 300–450 nm region, distinct from the native CD signal of the amino acids themselves (typically below 280 nm), further corroborates the ligand exchange and interactions between molecular capping ligands and nanocrystal surface.[45–47] As expected, L- and D-enantiomers of the amino acids induced mirror-image CD spectra in CdS QDs (Fig. S3–S5†).

The CD shape/sign, CD magnitude and CD anisotropy factor have been used to evaluate chirality of CdS QDs. CD an-

Table 1 Wavelengths of the lowest energy exciton peak (λ_{max}) of CdS QDs functionalized with chiral homologous amino acids (in MeOH) and the calculated CD anisotropy *g* factors

Capping ligand	λ_{max}/nm ($\Delta\lambda_{max}$ [a]/nm)	$g_{\lambda_{max}} \times 10^{-4}$ [b]	$g_{CD\ max} \times 10^{-4}$ [c] (λ, nm)
OA	419.4	—	—
L-Ser	420.4 (+1.2)	+1.2	−3.0 (392.5)
L-HomoSer	420.8 (+1.4)	+0.23	−1.2 (406.5)
L-Asp	419.0 (−0.4)	+0.21	−1.9 (386.0)
L-Glu	420.8 (+1.4)	−0.64	−1.3 (387.0)
L-Pro	420.0 (+0.6)	+0.09	−1.6 (397.0)
L-HomoPro	421.4 (+2.0)	+0.04	+1.1 (394.0)

[a] λ_{max} shifts relative to the OA-CdS (in cyclohexane). [b] CD anisotropy *g* factors at λ_{max}. [c] Maximum CD anisotropy g factors and the corresponding wavelengths.

isotropy values of amino acid capped CdS QDs are summarized in Table 1. The CD anisotropy factor (g), also known as Kuhn's dissymmetry ratio, is defined as $g = \Delta\varepsilon/\varepsilon = (A_L - A_R)/A$ where A represents the conventional absorbance and A_L and A_R are the absorptions of left and right circularly polarized light, respectively. This factor is a valuable tool for assessing the chirality of nanomaterials because it remains independent of both the concentration and the path length when the CD and absorbance spectra are measured on the same sample.

3.1 Ser-CdS and homoSer-CdS

Serine and homoserine each possess three electron donor functional groups: carboxylate, amino, and hydroxy. The additional methylene group in the side chain of homoserine shifts the hydroxy group from the C3 to the C4 position (Chart 1a). Consequently, the hydroxy group in homoserine is farther from both the surface anchoring carboxylate group and a quantum dot's surface compared to serine. This serine-homoserine pair is therefore ideal for studying the role of the hydroxy group (the third functional group attached to an achiral center) in ligand-induced QD chirality, as the anchoring carboxylate and C2 amino group positions remain constant. FTIR spectra of both L-Ser-CdS and L-homoSer-CdS showed symmetric and asymmetric carboxylate vibrations at approximately 1397 and 1566 cm^{-1}, respectively (Fig. S6†). The difference between the asymmetric and symmetric stretching frequencies, $\Delta\nu = \nu_{as}(OCO) - \nu_s(OCO)$, is a well-established empirical parameter for distinguishing between bridging, chelating, and unidentate binding modes of carboxylates to various metal complexes.[48,49] The observed difference ($\Delta\nu$ = 169 cm^{-1}) suggests a bridging binding mode, where both carboxylate oxygens interact with two positively charged cadmium atoms on the QD surface. Importantly, the Cd–O bonds between the cadmium atoms and the two oxygen atoms of the carboxylate are not necessarily identical.

Replacing oleic acid on the CdS surface with either L-Ser or L-homoSer resulted in minimal shifts of the lowest energy excitonic band ($\Delta\lambda_{max}$ < 1.4 nm, Table 1). The UV-Vis absorption spectra of L-Ser-CdS and L-homoSer-CdS exhibited nearly superimposing profiles ($\Delta\lambda_{max}$ = 0.4 nm, Fig. 1b). Similarly,

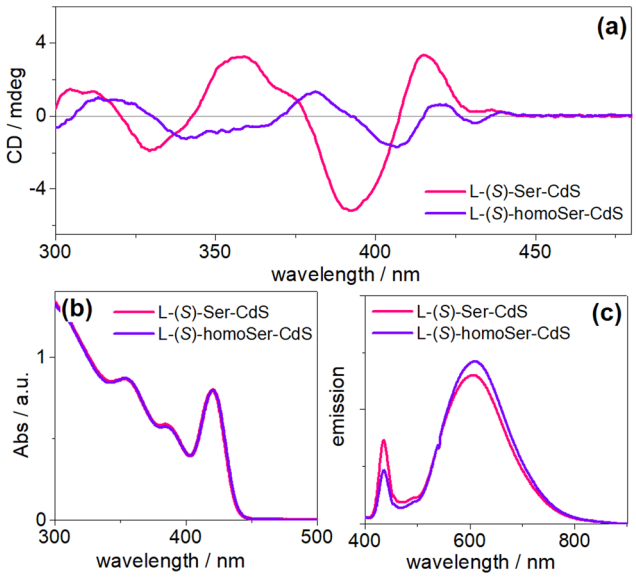

Fig. 1 (a) CD, (b) UV-Vis absorption, and (c) emission spectra (λ_{ex} = 355.0 nm) of CdS QDs functionalized with L-Ser (pink curve) and L-homoSer (violet curve) structural homologs. [CdS] ≈ 1.5 μM.

only small differences were observed in the emission spectra recorded under identical experimental conditions and parameters (λ_{ex} = 355.0 nm). Both spectra were dominated by deep trap emission (bands between 500 and 850 nm) with only small peaks at 435.5 nm resulting from band-edge emission (Fig. 1c). However, significant differences were observed in the shape and intensity of the circular dichroism (CD) spectra and the corresponding CD anisotropy (g) values. The CD spectrum of L-Ser-CdS (Fig. 1a, pink curve) exhibited a (+/−/+/−) profile between 450 and 325 nm (from longer to shorter wavelengths), with positive bands at 415 and 360 nm and negative bands at 390 and 330 nm. In contrast, the L-homoSer-CdS spectrum (Fig. 1a, violet curve) displayed a rather complex (−/+/−/+/−) pattern, with negative bands at 430, 410, and 340 nm and positive bands at 420 and 380 nm. Furthermore, L-Ser-CdS showed a nearly threefold higher CD anisotropy factor than L-homoSer-CdS ($g = -3.0 \times 10^{-4}$ *vs.* -1.2×10^{-4}, Table 1).

The significantly different CD spectra observed for L-Ser and L-homoSer bound to CdS QDs strongly indicate that the hydroxy group interacts with the CdS surface in at least one of these homologs. If binding were solely through carboxylate and amino groups, the CD profiles would be expected to be very similar.

We propose two possible explanations for the observed differences. First, the higher CD anisotropy for L-Ser-CdS may result from tridentate binding, where all three functional groups (carboxylate, amino, and hydroxy) simultaneously coordinate to the surface. In contrast, the additional methylene group in L-homoSer likely impedes effective interaction of the C4 hydroxy group with the surface, leading to weaker binding involving fewer functional groups. This could prevent a dominant binding geometry,[18,19] thereby reducing CD anisotropy.

Alternatively, the smaller footprint of tridentate-bound L-Ser than of tridentate-bound L-homoSer might enable closer packing on the CdS nanoparticle surface, resulting in higher surface coverage and enhanced ligand-induced anisotropy compared to the bulkier L-homoSer. Given the substantial differences in CD anisotropy and spectral shape, we consider the first explanation, involving differential hydroxy group interaction, to be the more likely contributor. Despite the near-identical absorption and emission spectra of L-Ser-CdS and L-homoSer-CdS, these CD data highlight the sensitivity of CD spectroscopy in discerning subtle variations in the surface binding geometries of chiral ligands and the resulting electronic states of ligand-nanocrystal coordination complexes.[20]

3.2 Asp-CdS and Glu-CdS QDs

Aspartic acid and glutamic acid (*i.e.*, homoaspartic acid) each possess three electron-donating functional groups (two carboxylate groups and an amino group). Previous experimental (FTIR) and calculation data suggest that biscarboxylic acids can bind to the surface *via* one or two carboxylate groups: C1 and C4 for L-Asp, and C1 and C5 for L-Glu (Chart 1b).[19,50–52] The extended carbon chain in glutamic acid increases the distance between its anchoring carboxylate groups and its larger conformation freedom, potentially leading to different binding geometries with the positively charged Cd atoms on the surface. Aspartic and glutamic acids have been shown to interact differently with $CuInS_2$/ZnS core/shell quantum dots, enabling selective detection of the former through fluorescence quenching, although the recognition mechanism has not been reported.[53] Functionalization of CdS with L-Asp resulted in a small blue shift of the lowest energy excitonic band ($\Delta\lambda_{max}$ = −0.4 nm), whereas L-Glu induced a larger red shift ($\Delta\lambda_{max}$ = +1.4 nm) compared to the OA-CdS (Table 1 and Fig. 2b). The fluorescence spectra (Fig. 2c, λ_{ex} = 355.0 nm) were dominated by deep trap emission within 500–800 nm spectral range with L-Asp-CdS yielding higher quantum yield than L-Glu-CdS. FTIR spectra confirmed CdS passivation by negatively charged carboxylates of Asp and Glu, showing ν_{as} and ν_s at approximately 1571 and 1387 for L-Asp and 1562 and 1395 cm^{-1} for L-Glu (Fig. S7†).

The induced CD spectra of L-Asp-CdS and L-Glu-CdS showed significant differences in the lowest energy excitonic band region (>400 nm), while exhibiting similar CD profiles below 400 nm. L-Asp-CdS displayed a (+/−) CD profile (from longer to shorter wavelength) above 370 nm, with a positive CD band at 410 nm and a negative CD band at 386 nm (Fig. 2a, pink curve). L-Glu-CdS displayed a more complex (+/−/+/−) pattern, with positive CD bands at 430 and 409 nm and negative CD bands at 419 and 388 nm (Fig. 2a, violet curve). Below 370 nm, the CD profiles of L-Asp-CdS and L-Glu-CdS were similar. As anticipated, comparable differences in the CD spectra were observed for the enantiomeric D-Asp-CdS and D-Glu-CdS QDs (Fig. S10†). As with Ser/homoSer, the larger CD anisotropy was calculated for the smaller L-Asp-CdS ($g_{CD} = -1.9 \times 10^{-4}$ at 386 nm *vs* $g_{CD} = -1.3 \times 10^{-4}$ at 387 nm; Table 1). The observed differences in CD spectra could be attributed to variations in the spatial arrangement of carboxylate groups. Conformational analysis revealed the following maximum distances between carboxylate oxygens (Fig. S9†): Asp exhibited distances of approximately 6.0 Å in the antiperiplanar conformation (extended chain) and 5.6 Å in the synclinal conformation. Glu displayed distances of approximately 7.3 Å (antiperiplanar) and 5.8 Å (synclinal, bent). Considering the two closed cadmium (Cd) atoms on the (111) CdS surface are separated by 4.16 Å and 7.21 Å, Glu can adopt a wider range of surface binding geometries compared to Asp. To further demonstrate the effect of ligand size, we also compared the CD spectra induced by the homologous *N*-acetylated derivatives of aspartic and glutamic acids (Chart 1b). The *N*-acetyl group has been selected because it has been shown to participate in multidentate surface binding with carboxylate groups.[18] As shown in Fig. 2d, homologous *N*-Ac-L-Asp and *N*-Ac-L-Glu exhibited very different CD spectra (in shape and intensity), supporting the hypothesis of different binding geometries and patterns resulting from the additional methylene group.

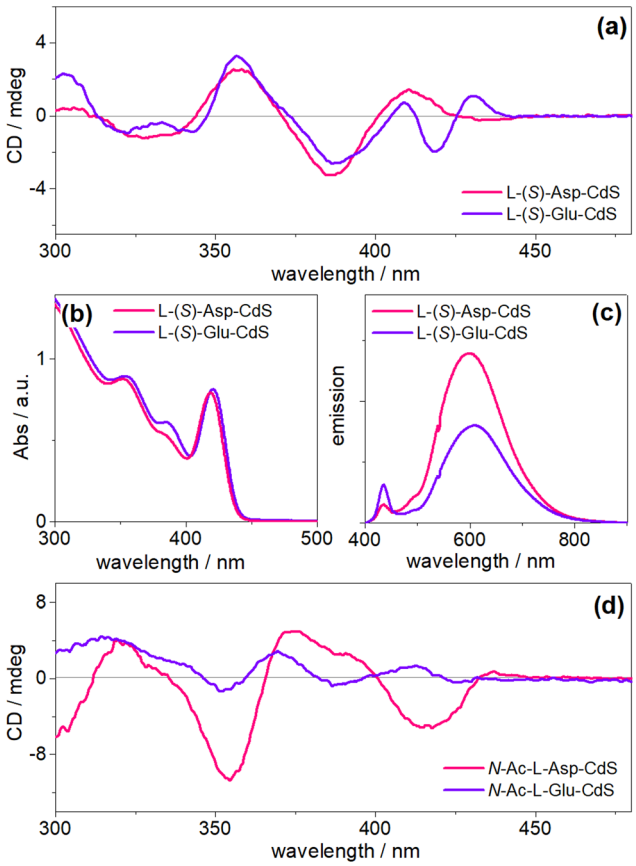

Fig. 2 (a) CD, (b) UV-Vis absorption, and (c) emission spectra (λ_{ex} = 355.0 nm) of CdS QDs functionalized with L-Asp (pink curve) and L-Glu (violet curve) structural homologs. (d) CD spectra of CdS QDs functionalized with *N*-Ac-L-Asp (pink curve) and *N*-Ac-L-Glu (violet curve). [CdS] ≈ 1.5 μM.

The different chiral ligand-quantum dot interactions between homologs are further emphasized by comparing the

CD spectra induced by L-Ser and L-Asp with those induced by L-homoSer and L-Glu. This comparison provides critical insights into the surface binding geometries and ligand–ligand patterns (Fig. 3). The similar CD spectra observed for L-Ser-CdS and L-Asp-CdS suggest comparable ligand surface orientations (similar footedness, Fig. 3a). Conversely, the one-carbon longer homologs, L-homoSer and L-Glu, likely display opposite surface pattern, as evidenced by the mirror-image-like CD spectra (Fig. 3b).[18,37–39]

3.3 Pro-CdS and homoPro-CdS QDs

Proline (Pro) possesses two electron-donating functional groups (carboxylate and imino) through which it can bind to the CdS surface (Chart 1c). Its C2 imino group, incorporated within a five-membered heterocyclic ring, makes it the most structurally rigid of the naturally occurring α-amino acids. Proline-passivated cobalt oxide/hydroxide nanoparticles (NPs), synthesized from cobalt(II) acetate and enantiopure proline, exhibited chirality due to proline-induced chiral distortions of the NP lattices.[54] L-Pro-ZnS QDs were used as a catalyst for the direct asymmetric aldol reaction with FTIR suggesting monodentate coordination of Pro with ZnS surface.[55] L-Pro has been successfully detected in solution by thioglycolic acid-capped CdTe quantum dots in the presence of other amino acids and metal cations *via* enhanced anodic electrochemiluminescence, though details on proline-QD interactions were not provided.[56] Pro has been shown to bind to metallic and metal oxide surfaces in vacuum, in its anionic form, primarily *via* the carboxylate group (typically *via* a bidentate coordination through the two carboxylate oxygens), although tridentate binding involving both the carboxylate and imino groups has also been reported.[23,57–59] Homoproline (pipecolic acid, homoPro; Chart 1c) shares the same number and positions of functional groups with Pro (C1 carboxylate and C2 imino groups), but differs in the size of its heterocyclic ring (six-membered *vs.* five-membered). Crystallographic studies reveal that homoPro exists as a zwitterion in a chair conformation with the carboxylate group occupying an equatorial position.[60] Given their structures, Pro and homoPro are well-suited for evaluating the effect of ligand size and shape on the induced CD of CdS QDs. Strong FTIR peaks at 1389 and 1580 cm^{-1} for L-Pro-CdS and at 1397 and 1582 cm^{-1} for L-homoPro-CdS were assigned to the symmetric and asymmetric COO^- stretching modes, confirming that L-Pro and L-homoPro are bound to the QD surface in their deprotonated form, likely *via* coordination through the two carboxylate oxygens (bridging binding mode to two cadmium atoms) and *via* the imino group (Fig. 4).

L-HomoPro induced a slightly larger red shift of the lowest energy excitonic band than L-Pro ($\Delta\lambda_{max}$ = 1.4 nm; Table 1), but L-Pro-CdS and L-homoPro-CdS exhibited nearly identical UV-Vis absorption spectra (Fig. 5b). Their emission spectra (λ_{ex} = 355.0 nm) were dominated by deep trap emission (bands

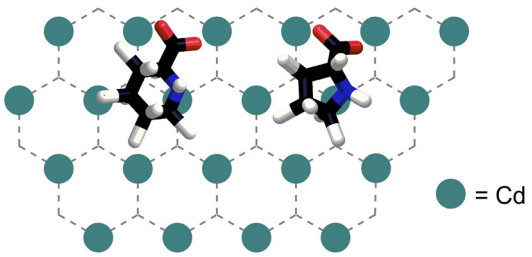

Fig. 4 Conceptual models depicting the distinct molecular footprints of L-homoPro (left) and L-Pro (right) on the (111) CdS surface (zinc blende), illustrating binding *via* carboxylate and imino groups.

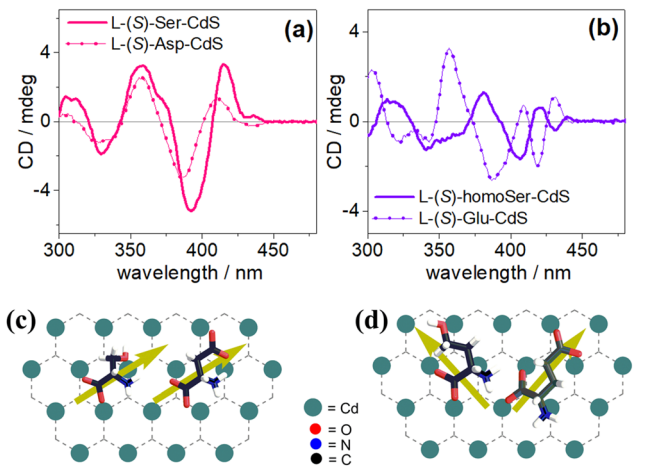

Fig. 3 CD spectra of (a) L-Ser-CdS and L-Asp-CdS QDs and (b) L-homoSer-CdS and L-Glu-CdS. [CdS] ≈ 1.5 μM. Conceptual representation of multidentate surface binding on the (111) CdS surface (zinc blende), showing: (c) similar surface orientation (footedness) for L-Ser and L-Asp; (d) opposite surface orientation for L-homoSer and L-Glu.

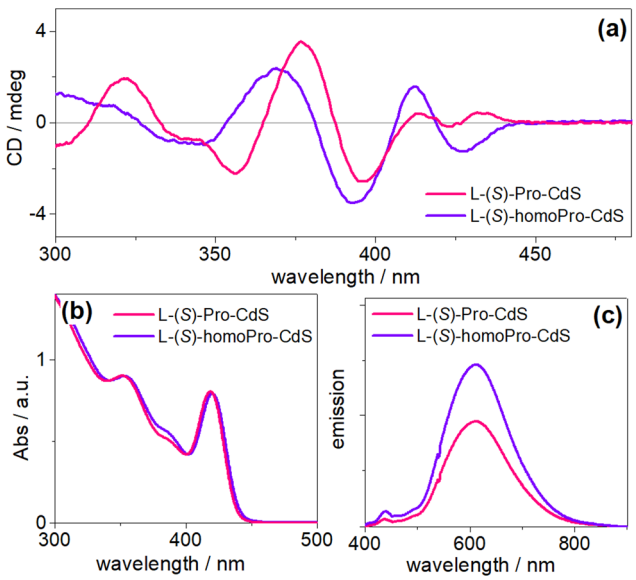

Fig. 5 (a) CD spectra and (b) UV-Vis absorption spectra, and (c) emission spectra (λ_{ex} = 355.0 nm) of CdS QDs functionalized with L-Pro (pink curve) and L-homoPro (violet curve) structural homologs. [CdS] ≈ 1.5 μM.

between 500 and 850 nm, Fig. 5c) and differed in quantum yield but not the emission wavelengths. The CD spectrum of L-Pro-CdS (Fig. 4a, pink curve) exhibited a very weak trisignate CD signal in the lowest energy excitonic band, whereas L-homoPro-CdS (Fig. 5a, violet curve) displayed a strong bisignate CD signal (a negative CD band at 427 nm and a positive CD band at 412 nm). Although similar (−/+/−) CD profiles were observed for both L-Pro-CdS and L-homoPro-CdS between 330 and 410 nm, the individual CD bands appeared at different wavelengths and with different intensities. As predicted, analogous differences in the CD spectra were observed for the enantiomeric D-Pro-CdS and D-homoPro-CdS QDs. Once again, CD anisotropies calculated for the smaller L-Pro (g_{CD} = +1.6 × 10^{-4} at 397.0 nm; Table 1) were higher than for the bulkier L-homoPro (g_{CD} = +1.1 × 10^{-4} at 394.0 nm). In summary, the CD spectra highlighted that, even with identical position and type of surface binding groups and similar surface binding, the structural differences between Pro and homoPro (specifically the bulkiness, conformational rigidity, and lateral repulsion of their ring structures) resulted in distinct induced CD spectra of CdS QDs.

4. Conclusions

We reported the initial study investigating the influence of capping ligand size on the ligand-induced circular dichroism (CD) of CdS QDs using pairs of amino acids with different side chain length. Functionalization of CdS QDs with homologous amino acid pairs (Ser/homoSer, Asp/Glu, and Pro/homoPro) demonstrated that the capping ligand size, the presence of the third functional group (attached to the achiral carbon) and the distance between the anchoring carboxylate group and the third functional group, all significantly impacted the shape and magnitude of the induced CD spectrum. In all three cases, the smaller, sterically less demanding capping ligand induce larger CD anisotropy than its bulkier counterpart. The Pro/homoPro pair provides compelling evidence that the size of the molecule itself can effectively tune the induced CD signal of QDs. The impact of replacing a carboxylate group with a hydroxy group on the induced CD signal is primarily determined by the distance between the primary anchoring group and the secondary functional group, rather than the exact chemistries of the functional groups, and these CD spectral changes (including CD signal inversion) can be correlated with the ligand's surface binding geometry and ligand–ligand surface patterns (*i.e.*, ligand "footedness"). Our data also underscored the crucial role that the CD spectroscopy plays in probing subtle differences in the binding geometries of chiral organic capping ligands on the surface of nanocrystals. Identifying the structural factors that influence chirality induction in QDs would facilitate better control of their properties and potentially enable the rational design of materials with desirable, tunable chiroptical properties.

Data availability

All data that support the findings of this study are included within the article and the ESI.†

Conflicts of interest

There are no conflicts to declare.

Acknowledgements

This work was supported by the University of New Hampshire (K. V.). M. B. thanks Yonsei University. We thank Yuri Kwon (UNH) for assistance with OA-CdS QDs. K. V. acknowledges that this material is partially based upon work conducted while serving at National Science Foundation (NSF). Any opinions, findings, and conclusions or recommendations expressed in this material are those of the authors and do not necessarily reflect the views of NSF.

References

1 M. P. Moloney, Y. K. Gun'ko and J. M. Kelly, *Chem. Commun.*, 2007, 3900–3902, DOI: 10.1039/b704636g.
2 U. Tohgha, K. K. Deol, A. G. Porter, S. G. Bartko, J. K. Choi, B. M. Leonard, K. Varga, J. Kubelka, G. Muller and M. Balaz, *ACS Nano*, 2013, **7**, 11094–11102.
3 U. Tohgha, K. Varga and M. Balaz, *Chem. Commun.*, 2013, **49**, 1844–1846.
4 M. Sun, L. Xu, A. Qu, P. Zhao, T. Hao, W. Ma, C. Hao, X. Wen, F. M. Colombari, A. F. de Moura, N. A. Kotov, C. Xu and H. Kuang, *Nat. Chem.*, 2018, **10**, 821–830.
5 D. Wawrzyńczyk, J. Szeremeta, M. Samoć and M. Nyk, *Sens. Actuators, B*, 2017, **252**, 483–491.
6 I. V. Martynenko, V. A. Kuznetsova, I. K. Litvinov, A. O. Orlova, V. G. Maslov, A. V. Fedorov, A. Dubavik, F. Purcell-Milton, Y. K. Gun'ko and A. V. Baranov, *Nanotechnology*, 2016, **27**, 075102.
7 V. A. Kuznetsova, A. K. Visheratina, A. Ryan, I. V. Martynenko, A. Loudon, C. M. Maguire, F. Purcell-Milton, A. O. Orlova, A. V. Baranov, A. V. Fedorov, A. Prina-Mello, Y. Volkov and Y. K. Gun'Ko, *Chirality*, 2017, **29**, 403–408.
8 X. Wang, J. Hao, J. Cheng, J. Li, J. Miao, R. Li, Y. Li, J. Li, Y. Liu, X. Zhu, Y. Liu, X. W. Sun, Z. Tang, M.-H. Delville, T. He and R. Chen, *Nanoscale*, 2019, **11**, 9327–9334.
9 J. Yeom, B. Yeom, H. Chan, K. W. Smith, S. Dominguez-Medina, J. H. Bahng, G. Zhao, W.-S. Chang, S.-J. Chang, A. Chuvilin, D. Melnikau, A. L. Rogach, P. Zhang, S. Link, P. Král and N. A. Kotov, *Nat. Mater.*, 2015, **14**, 66–72.
10 B. P. Bloom, V. Kiran, V. Varade, R. Naaman and D. H. Waldeck, *Nano Lett.*, 2016, **16**, 4583–4589.
11 B. P. Bloom, B. M. Graff, S. Ghosh, D. N. Beratan and D. H. Waldeck, *J. Am. Chem. Soc.*, 2017, **139**, 9038–9043.

12 X. Gao, B. Han, X. Yang and Z. Tang, *J. Am. Chem. Soc.*, 2019, **141**, 13700–13707.
13 V. Kuznetsova, Y. Gromova, M. Martinez-Carmona, F. Purcell-Milton, E. Ushakova, S. Cherevkov, V. Maslov and Y. K. Gun'ko, *Nanophotonics*, 2021, **10**, 797–824.
14 Y. H. Kwon, S. Tannir, M. Balaz and K. Varga, *Chirality*, 2022, **34**, 70–76.
15 X. Wen, H. Fan, L. Jing, M. Deng, X. Huang, T. Jiao, L. Zhang and M. Liu, *Mater. Adv.*, 2022, **3**, 682–688.
16 K. Ngamdee and W. Ngeontae, *Sens. Actuators, B*, 2018, **274**, 402–411.
17 F. Yang, G. Gao, J. Wang, R. Chen, W. Zhu, L. Wang, Z. Ma, Z. Luo and T. Sun, *J. Colloid Interface Sci.*, 2019, **537**, 422–430.
18 J. K. Choi, B. E. Haynie, U. Tohgha, L. Pap, K. W. Elliott, B. M. Leonard, S. V. Dzyuba, K. Varga, J. Kubelka and M. Balaz, *ACS Nano*, 2016, **10**, 3809–3815.
19 K. Varga, S. Tannir, B. E. Haynie, B. M. Leonard, S. V. Dzyuba, J. Kubelka and M. Balaz, *ACS Nano*, 2017, **11**, 9846–9853.
20 A. Ben-Moshe, A. Teitelboim, D. Oron and G. Markovich, *Nano Lett.*, 2016, **16**, 7467–7473.
21 A. S. Baimuratov, I. D. Rukhlenko, Y. K. Gun'ko, A. V. Baranov and A. V. Fedorov, *Nano Lett.*, 2015, **15**, 1710–1715.
22 M. V. Mukhina, V. G. Maslov, A. V. Baranov, A. V. Fedorov, A. O. Orlova, F. Purcell-Milton, J. Govan and Y. K. Gun'ko, *Nano Lett.*, 2015, **15**, 2844–2851.
23 M. Forster, M. S. Dyer, M. Persson and R. Raval, *J. Am. Chem. Soc.*, 2009, **131**, 10173–10181.
24 G. Li, X. Fei, H. Liu, J. Gao, J. Nie, Y. Wang, Z. Tian, C. He, J.-L. Wang, C. Ji, D. Oron and G. Yang, *ACS Nano*, 2020, **14**, 4196–4205.
25 P. Han, T. Du, X. Yang, Y. Zhao, S. Zhou and J. Zhao, *J. Phys. Chem. Lett.*, 2024, **15**, 3249–3257.
26 D. Chabeda, S. Gee and E. Rabani, *J. Phys. Chem. Lett.*, 2024, **15**, 7863–7869.
27 Y. Zhou, M. Yang, K. Sun, Z. Tang and N. A. Kotov, *J. Am. Chem. Soc.*, 2010, **132**, 6006–6013.
28 A. Forde, D. Ghosh, D. Kilin, A. C. Evans, S. Tretiak and A. J. Neukirch, *J. Phys. Chem. Lett.*, 2022, **13**, 686–693.
29 Y. A. Joh, Y. H. Kwon, S. Tannir, B. M. Leonard, J. Kubelka, K. Varga and M. Balaz, *J. Mater. Chem. C*, 2021, **9**, 17483–17495.
30 M. Puri and V. E. Ferry, *ACS Nano*, 2017, **11**, 12240–12246.
31 X. Shao, Y. Wu, S. Jiang, B. Li, T. Zhang and Y. Yan, *J. Mater. Chem. C*, 2021, **9**, 555–561.
32 Y. H. Kwon, Y. A. Joh, B. M. Leonard, M. Balaz and K. Varga, *J. Colloid Interface Sci.*, 2023, **642**, 771–778.
33 Y. Wu, X. Shao, Y. Zhou, S. Jiang, T. Y. Zhang and Y. Yan, *Nanotechnology*, 2021, **32**, 375701.
34 J. Kuno, T. Kawai and T. Nakashima, *Nanoscale*, 2017, **9**, 11590–11595.
35 V. A. Kuznetsova, E. Mates-Torres, N. Prochukhan, M. Marcastel, F. Purcell-Milton, J. O'Brien, A. K. Visheratina, M. Martinez-Carmona, Y. Gromova, M. Garcia-Melchor and Y. K. Gun'ko, *ACS Nano*, 2019, **13**, 13560–13572.
36 L. Branzi, F. Purcell-Milton, C. Cressoni, M. Back, E. Cattaruzza, A. Speghini, Y. K. Gun'ko and A. Benedetti, *Nanoscale*, 2022, **14**, 12174–12182.
37 Z. N. Georgieva, Z. Zhang, P. Zhang, B. P. Bloom, D. N. Beratan and D. H. Waldeck, *J. Phys. Chem. C*, 2022, **126**, 15986–15995.
38 J. Kuno, Y. Imamura, M. Katouda, M. Tashiro, T. Kawai and T. Nakashima, *Angew. Chem., Int. Ed.*, 2018, **57**, 12022–12026.
39 J. Guo, Z. L. Zhao, R. Sun, Y. L. Zhou and X. Q. Gao, *ACS Appl. Nano Mater.*, 2024, **7**, 16894–16900.
40 W. W. Yu, L. Qu, W. Guo and X. Peng, *Chem. Mater.*, 2003, **15**, 2854–2860.
41 B. Fritzinger, R. K. Capek, K. Lambert, J. C. Martins and Z. Hens, *J. Am. Chem. Soc.*, 2010, **132**, 10195–10201.
42 P. K. Tamukong, W. D. N. Peiris and S. Kilina, *Phys. Chem. Chem. Phys.*, 2016, **18**, 20499–20510.
43 D. A. Kurtina, V. B. Zaytsev and R. B. Vasiliev, *Materials*, 2024, **17**, 237.
44 O. Voznyy, *J. Phys. Chem. C*, 2011, **115**, 15927–15932.
45 L. I. Katzin and E. Gulyas, *J. Am. Chem. Soc.*, 1968, **90**, 247–251.
46 H. Nishino, A. Kosaka, G. A. Hembury, K. Matsushima and Y. Inoue, *J. Chem. Soc., Perkin Trans. 2*, 2002, 582–590.
47 N. Amdursky and M. M. Stevens, *ChemPhysChem*, 2015, **16**, 2768–2774.
48 A. Y. Koposov, T. Cardolaccia, V. Albert, E. Badaeva, S. Kilina, T. J. Meyer, S. Tretiak and M. Sykora, *Langmuir*, 2011, **27**, 8377–8383.
49 M. Kakihana, T. Nagumo, M. Okamoto and H. Kakihana, *J. Phys. Chem.*, 1987, **91**, 6128–6136.
50 Z. Wang, Y. Yang, T. Zou, X. Xing, R. Zhao and Y. Wang, *J. Phys. Chem. Solids*, 2020, **136**, 109160.
51 Z. Wang, X. Xiao, Y. Yang, T. Zou, X. Xing, R. Zhao, Z. Wang and Y. Wang, *Nanomaterials*, 2019, **9**, 1165.
52 J. Heo and C.-S. Hwang, *Nanomaterials*, 2016, **6**, 82.
53 S. Safari, A. Amiri and A. Badiei, *Spectrochim. Acta, Part A*, 2023, **291**.
54 Y. Yamagiwa, M. Harada and H. Yao, *J. Phys. Chem. C*, 2022, **126**, 21308–21318.
55 E. Shah and H. P. Soni, *RSC Adv.*, 2013, **3**, 17453–17461.
56 M. Zhang, F. W. Wan, S. W. Wang, S. G. Ge, M. Yan and J. H. Yu, *J. Lumin.*, 2012, **132**, 938–943.
57 G. J. Fleming, K. Adib, J. A. Rodriguez, M. A. Barteau, J. M. White and H. Idriss, *Surf. Sci.*, 2008, **602**, 2029–2038.
58 S. Dutta and A. J. Gellman, *Chirality*, 2020, **32**, 200–214.
59 M. Sowmiya and K. Senthilkumar, *Theor. Chem. Acc.*, 2015, **135**, 12.
60 S. K. Bhattacharjee and K. K. Chacko, *Acta Crystallogr., Sect. B*, 1979, **35**, 396–398.

